Magnetic order in 2p-electron systems: Electron paramagnetic resonance and antiferromagnetic resonance in the alkali hyperoxides KO_2, RbO_2, and CsO_2

M. Labhart,* D. Raoux,† and W. Känzig
Laboratory of Solid State Physics, Swiss Federal Institute of Technology, CH-8093 Zürich, Switzerland

M. A. Bösch‡
Laboratory of Atomic and Solid State Physics, Cornell University, Ithaca, New York 14853
(Received 20 November 1978)

The low-temperature phases of the alkali hyperoxides KO_2, RbO_2, and CsO_2 have been investigated by means of electron paramagnetic resonance (EPR) and antiferromagnetic resonance (AFMR). The knowledge of their structural and magnetic properties could be enlarged substantially. The orientation of the O_2^- molecule ions in the phases IV and V of KO_2 was determined accurately. It changes considerably at the phase transition IV $\rightleftarrows$ V (11 K). For KO_2, RbO_2, and CsO_2 the experimental results are compatible with antiferromagnetic order at low temperatures. The magnetic properties are discussed within the framework of a mean-field approximation. The pertinent parameters describing the spin-spin interactions were determined for RbO_2 and CsO_2 and some of them for KO_2 using the Néel temperature, the Curie-Weiss temperature, the spin-flop field, the temperature dependence of the EPR resonance field, and the AFMR frequencies. In RbO_2 and CsO_2 the anisotropy of the mean-field parameters originates predominantly in the anisotropic exchange interaction. The combination of electron paramagnetic resonance and antiferromagnetic resonance data yields information about the magnetic structure: The easy axis of magnetization is perpendicular to the internuclear axis of the O_2^- ions, and the hard axis is parallel to it for all three compounds.

I. INTRODUCTION

The alkali hyperoxides are ionic crystals consisting of alkali ions and O_2^- molecule ions. There exists detailed knowledge of the O_2^- ion substituting for a halide ion in alkali halides deduced from EPR and optical spectroscopy.[1-3] The ground state $^2\Pi_g$ is paramagnetic. Even a thorough study of the magnetic and elastic interactions between the partners of pairs of O_2^- centers is available.[4,5]

In the alkali hyperoxides the interactions between the O_2^- molecule ions give rise to many phase transitions involving changes of the orientation pattern[6] and of the magnetic properties.[7] Neutron-diffraction experiments show that KO_2 orders antiferromagnetically below 7 K.[8] Measurements of the magnetic susceptibility[7] and the electron-paramagnetic-resonance (EPR) and antiferromagnetic-resonance (AFMR) data reported in the present work indicate that RbO_2 and CsO_2 also order antiferromagnetically below 15 and 9.6 K, respectively. In NaO_2 evidence for magnetic short-range order was reported.[6] Thus, the alkali hyperoxides are among the rare substances exhibiting magnetic order of 2p electrons.[9] Another example is solid oxygen with a Néel temperature $T_N = 23.9$ K.[10] The present knowledge of the crystallographic changes occuring at the different phase transitions is summarized in Sec. II.

The aim of the present investigation is to gain a detailed knowledge of the orientation of the internuclear axis of the O_2^- ions, of the magnetic interactions, and of the magnetic structure in KO_2, RbO_2, and CsO_2. The results of a comprehensive single-crystal EPR study and of an AFMR study are reported. The g tensor yields the orientation of the O_2^- molecules with a much higher accuracy than x-ray data. The EPR linewidth, the EPR resonance fields, and the AFMR frequencies give information about the spin-spin interactions. The magnetic structure is probed by AFMR.

II. CRYSTAL STRUCTURES

The structures of the different phases of the alkali hyperoxides are described comprehensively in Refs. 6 and 11. Figure 1 gives a survey over KO_2, RbO_2, and CsO_2. The average (symmetrized) structure of the room-temperature phase (phase II) of all three hyperoxides is tetragonal and of the CaC_2-type [Fig. 2(a)]. The actual structure, however, has orthorhombic symmetry. Due to the Jahn-Teller effect the O_2^- molecule ions cannot assume the symmetrical position they would have in the ideal CaC_2-type structure.[12] They are tilted and/or displaced in a

KO_2	RbO_2	CsO_2
II average structure tetragonal: CaC_2 - type (fig. 2a) 2 orthorhombic domains	II (as KO_2 II)	II (as KO_2 II)
231 K	194 K	190 K
III incommensurate superstructure orthorhombic	III incommensurate superstructure α pseudotetragonal	III incommensurate superstructure orthorhombic
196 K		
IV monoclinic (fig. 2b) 4 domains	β orthorhombic	
10.6-12.1 K (hysteresis)	γ weakly monoclinic	
V coexistence of the crystallographic structures of phases IV and VI	15.1 K	
7.1 K	IV	9.6 K
VI triclinic 8 crystallographic domains antiferromagnetic	14.7 K	IV orthorhombic (as III)
	V weakly monoclinic (as III γ) antiferromagnetic	antiferromagnetic

FIG. 1. Survey over the structures of the low-temperature phases of KO_2, RbO_2, and CsO_2.

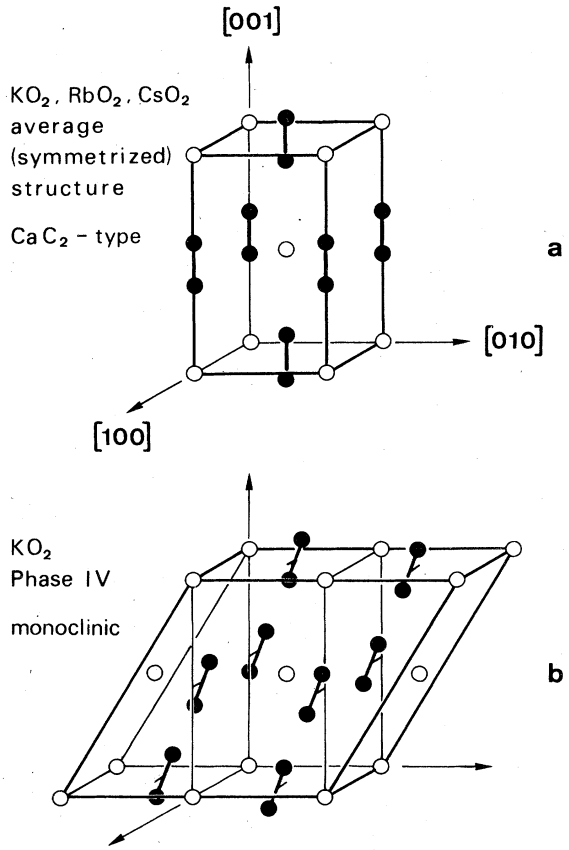

FIG. 2. Crystallographic structures.

more or less ordered fashion. In phase III there is a strong correlation between the O_2^- molecules with respect to tilt and displacement. X-ray diffraction patterns indicate an incommensurate superstructure. In CsO_2 this structure persists upon cooling into the antiferromagnetic phase IV. In RbO_2 a slight monoclinic distortion appears at lower temperatures (phase III γ). A change in the crystallographic structure from phase III γ to the antiferromagnetic phase V was not observed.

KO_2 behaves differently. The monoclinic phase IV seems to be completely ordered crystallographically except for the existence of domains. The molecules are tilted and displaced as shown in Fig. 2(b). (The correct crystallographic cell has the double volume of the CaC_2-type cell.) In phase V the crystallographic structures of the phases IV and VI coexist. The structure of phase VI arises from that of phase IV by a distortion of the monoclinic cell and a reorientation of the O_2^- molecules.

All these structures can be derived from the tetragonal CaC_2-type structure through a slight distortion of the cell combined with an appropriate tilting and displacement pattern of the molecules. The tetragonal CaC_2-type structure can be regarded as a crude average structure in all phases. Its axes will be taken as reference system throughout this paper.

III. MEAN-FIELD APPROXIMATION

The magnetic interactions will be discussed within the framework of a mean-field approximation (MFA).

a. The relation between the mean-field parameters and the microscopic interactions. For the alkali hyperoxides the spin Hamiltonian can be written

$$\mathcal{H}=\sum_{j<k}(J_{jk}\vec{S}_j\cdot\vec{S}_k+\vec{S}_j\cdot\vec{J}'_{jk}\cdot\vec{S}_k)+g_0\mu_B\vec{H}\cdot\sum_j\vec{S}_j \quad , \tag{1}$$

where $\mathrm{Tr}\vec{J}'_{jk}=0$. $\vec{H}=(1/g_0)\,\vec{g}\cdot\vec{H}_{ex}$ is the reduced field and $\vec{H}_{ex}$ the externally applied field. g_0 designates the free-electron g value, and μ_B the Bohr magneton. The dipole-dipole interaction is included in the J's. The signs have been chosen so that J_{jk} is positive for antiferromagnetic coupling. Because $S=\frac{1}{2}$ there is no single-ion anisotropy ($\vec{J}'_{jj}=0$). For a two-sublattice antiferromagnet the energy is then

$$\begin{aligned}E=&A\vec{M}_A\cdot\vec{M}_B+\tfrac{1}{2}\Gamma(\vec{M}_A{}^2+\vec{M}_B{}^2)+\vec{M}_A\cdot\vec{A}'\cdot\vec{M}_B\\&+\tfrac{1}{2}(\vec{M}_A\cdot\vec{\Gamma}'\cdot\vec{M}_A+\vec{M}_B\cdot\vec{\Gamma}'\cdot\vec{M}_B)\\&-\vec{H}\cdot(\vec{M}_A+\vec{M}_B) \quad ,\end{aligned} \tag{2}$$

where $\vec{M}_A=-Ng_0\mu_B\langle\vec{S}_A\rangle$ and $\vec{M}_B=-Ng_0\mu_B\langle\vec{S}_B\rangle$ are the reduced magnetizations of the sublattices A and B, respectively. N is the number per volume of spins on one sublattice. The mean-field parameters A, Γ, $\vec{A}'$, and $\vec{\Gamma}'$ are

$$A=\frac{1}{Ng_0^2\mu_B^2}\left(\sum_{k\in B}J_{jk}\right)_{j\in A} \quad , \tag{3a}$$

$$\vec{A}'=\frac{1}{Ng_0^2\mu_B^2}\left(\sum_{k\in B}\vec{J}'_{jk}\right)_{j\in A} \tag{3b}$$

[one picks out a ion j of the sublattice A (or B) and sums over all ions k of the other sublattice B (or A)];

$$\Gamma=\frac{1}{Ng_0^2\mu_B^2}\left(\sum_{k\in A}J_{jk}\right)_{j\in A} \quad , \tag{3c}$$

$$\vec{\Gamma}'=\frac{1}{Ng_0^2\mu_B^2}\left(\sum_{k\in A}\vec{J}'_{jk}\right)_{j\in A} \tag{3d}$$

[one picks out a ion j of the sublattice A (or B) and sums over all other ions k in the same sublattice]. The A's represent the interactions between the two different sublattices whereas the Γ's represent the interactions within the same sublattice.

b. The orthorhombic approximation. CsO_2 is orthorhombic down to the lowest temperatures, and in RbO_2 the distortion from orthorhombicity is small ($\gamma=90.7°$).[11] We therefore assume the principal axes of the tensors $\vec{A}'$, $\vec{\Gamma}'$, and $\vec{g}$ to be parallel to each other. This assumption cannot be justified in the phases IV, V, and VI of KO_2, where the deviation from orthorhombic symmetry is larger. Nevertheless we have to use it in order to reduce the number of parameters. The tensors $\vec{P}$ and $\vec{Q}$ defined by

$$\vec{P}=\vec{A}'+\vec{\Gamma}' \quad \text{and} \quad \vec{Q}=\vec{A}'-\vec{\Gamma}' \tag{4}$$

will be frequently used. Their principal values are designated by P_α and Q_α ($\alpha=x,y,z$). x shall denote the easy and z the hard axis so that $Q_x>Q_y>Q_z$.

The Néel temperature T_N is given by

$$\begin{aligned}T_N&=\frac{Ng_0^2\mu_B^2S(S+1)}{3k_B}(A-\Gamma+Q_x)\\&=\tfrac{1}{2}C(A-\Gamma+Q_x) \quad .\end{aligned} \tag{5}$$

The paramagnetic Curie-Weiss temperature Θ_α for the magnetic field applied along the principal axis α ($\alpha=x,y,z$) is

$$\begin{aligned}\Theta_\alpha&=-\frac{Ng_0^2\mu_B^2S(S+1)}{3k_B}(A+\Gamma+P_\alpha)\\&=-\tfrac{1}{2}C(A+\Gamma+P_\alpha) \quad .\end{aligned} \tag{6}$$

We calculate the *isotropic mean-field parameters* A and Γ using the experimental values for T_N and Θ from Ref. 7 thereby neglecting the anisotropic mean-field parameters. N is obtained from the volume of the unit cell given in Ref. 11. The results are summarized in Table I.

c. The anisotropy of the mean-field parameters originates completely in the anisotropy of the exchange

TABLE I. Experimental Néel and Curie-Weiss temperatures of KO_2, RbO_2, and CsO_2 (Ref. 7) and the resulting isotropic-mean-field parameters.

	T_N (K)	Θ (K)	A	Γ
KO_2	7.1	−16 (phase V)	1.97×10^3	0.76×10^3
RbO_2	15	−26 (phase III)	3.92×10^3	1.05×10^3
CsO_2	9.6	−28 (phase III)	4.32×10^3	2.11×10^3

interaction and the dipole-dipole interaction because no single-ion anisotropy is present. The order of magnitude of the anisotropic part of the exchange interaction J_A can be estimated using the relation

$$J_A \approx (\Delta g/g)^2 J \ , \tag{7}$$

given by Moriya,[13] where J is the isotropic exchange interaction and $\Delta g = g - g_0$. From the experimental fact $(\Delta g/g)^2 << 1$ one concludes that the principal values of the tensors $\vec{A}'$ and $\vec{\Gamma}'$ are much smaller than the isotropic mean-field parameters A and Γ. Theory predicts then for an antiferromagnet spin-flop behavior.[14] Thus the alkali hyperoxides do not undergo a metamagnetic phase transition refuting earlier proposals for KO_2.[7] However, this reference reports an anomaly in the adiabatic differential susceptibility at fields of about 25, 26, and 28 kG in KO_2, RbO_2, and CsO_2, respectively, which disappears above the Néel temperature. It can now be interpreted as the spin-flop transition. According to the MFA the reduced spin-flop field H_c at $T = 0$ K, neglecting $\vec{A}'$ and $\vec{\Gamma}'$ with respect to A, is

$$H_c = [2(Q_x - Q_y) A M_0^2]^{1/2} \ , \tag{8}$$

where

$$M_0 = |\vec{M}_A| = |\vec{M}_B| = N g_0 \mu_B S \ .$$

In this way $Q_x - Q_y$ can be determined using experimental data. $Q_x - Q_z$ is obtained from AFMR and the tensor $\vec{P}$ from the temperature dependence of the EPR resonance field. Numerical data will be given in Secs. IV and V.

IV. ELECTRON PARAMAGNETIC RESONANCE

A. Experimental techniques

All EPR spectra were taken with a Q-band spectrometer using balanced mixer detection and cylindrical microwave cavities (TE_{011} and TE_{012}) immersed in helium gas in order to establish thermal contact to the sample and to the liquid helium bath. The cavity carried an electric heater in order to attain temperatures above the bath temperature. A carbon resistor and a copper-constantan thermocouple fixed to the top of the cavity served as thermometers. Due to microwave heating the sample temperature could be as much as one degree above the temperature of the thermometers as was checked using the known phase transition temperatures. In the figures the temperature indicated by the thermometers is given. All EPR measurements with the exception of most intensity measurements of KO_2 were made using single crystals grown in liquid ammonia as described in Ref. 15. The strongly hygroscopic samples were permanently sealed in Lindemann-glass tubes in an atmosphere of dry helium gas. The crystals were oriented at room temperature by x-ray Laue photographs and afterwards transferred to the microwave cavity. Only samples with sharp diffraction spots were used. For the resonance field the center between the extrema of the first derivative of the absorption line was taken. Polycrystalline DPPH (α, α'-diphenyl-β-picryl hydrazyl) [$g = 2.0032$ at helium temperatures (see Ref. 16)] served as a g standard.

B. KO_2

1. Intensity

Figure 3 shows the temperature dependence of the intensity of the paramagnetic resonance absorption in the range from 5 to 140 K. Below 7 K the intensity decreases rapidly, which confirms the onset of antiferromagnetic order. The phase transition IV ↔ V manifests itself by a jump. This is also observed in the static susceptibility.[7] Above 100 K the linewidth increases rapidly with increasing temperature thus reducing the accuracy of the integration. The deviation from the Curie-Weiss law above 100 K may be due to an underestimation of the intensity in the wings of the line. The absolute number of absorbing spins has been determined by comparing the intensity of the KO_2 absorption to that of a DPPH sample, which in turn was calibrated against a $CuSO_4 \cdot 5H_2O$ sample of known mass. The number of spins determined from the Curie-Weiss law below 80 K turned out to be equal to the number of O_2^- ions calculated from the weight of the sample within the experimental accuracy of about 20%. This proves that the detected signal is due to the O_2^- ions constituting the crystal.

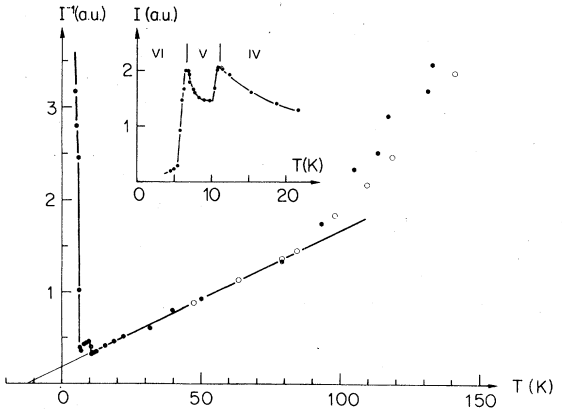

FIG. 3. Temperature dependence of the intensity I of the paramagnetic resonance absorption of KO_2 (arbitrary units). Full circles: polycrystalline sample. Open circles: single crystal.

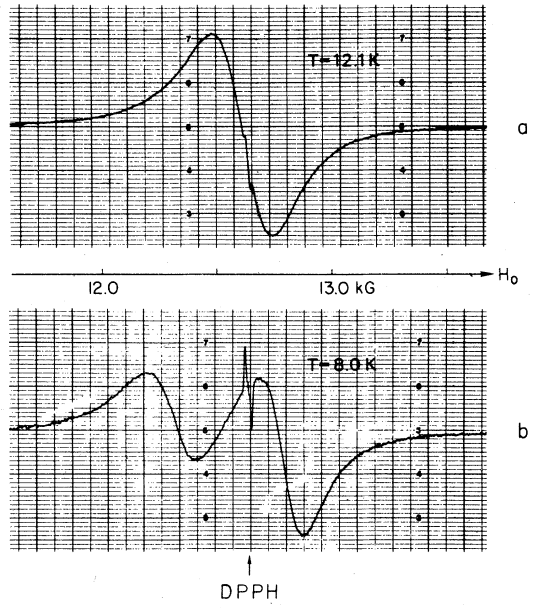

FIG. 4. EPR spectra of a single crystal of KO_2 for the static magnetic field along the [110] axis of the average tetragonal CaC_2-type cell. $\nu = 35.4$ GHz. (a) $T = 12.1$ K (phase IV) and (b) $T = 8.0$ K (phase V).

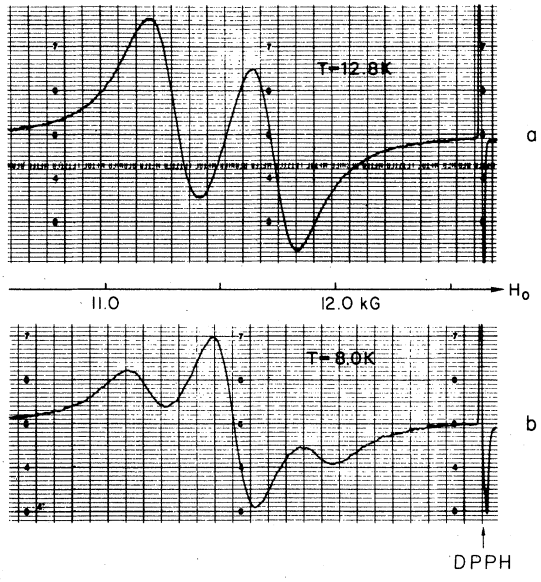

FIG. 5. EPR spectra of a single crystal of KO_2 for the static magnetic field in a (110) plane of the average tetragonal CaC_2-type cell, including an angle Φ with the [001] axis. $\nu = 35.4$ GHz. (a) $T = 12.8$ K (phase IV), $\Phi = 20.3°$ and (b) $T = 8.0$ K (phase V), $\Phi = 18.3°$.

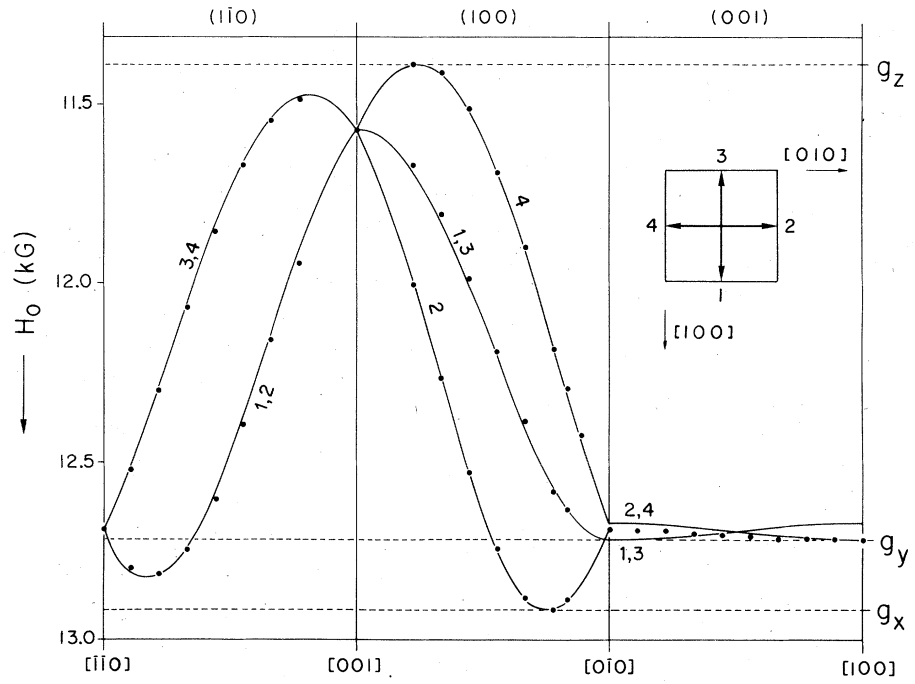

FIG. 6. Angular dependence of the resonance fields in KO_2 IV at $T = 13.0$ K for different planes (measurements of crystal No. 11). The solid lines are the calculated resonance fields based on the model described in the text. $\nu = 35.4$ GHz.

2. *Orientation of the principal axes of the g tensor; crystallographic domains*

Only between 7 K and about 100 K (phases IV and V) the single-crystal spectra were intense enough and the lines narrow enough to permit an accurate investigation. Typical spectra are given in Figs. 4 and 5. For the determination of the orientation of the principal axes of the g tensor the angular variation of the resonance fields was studied for different crystal planes.

Figure 6 represents the data for the monoclinic phase IV at $T=13.0$ K. X-ray data[17] give the symmetry of the unit cell and the domain structure. There are four domain orientations, which transform into each other by 90° rotations around the [001] axis of the average tetragonal structure. For a general crystal orientation one thus expects four EPR lines. For the special planes investigated some of these either coincide or cannot be resolved, as indicated in Fig. 6. The point symmetry of an O_2^- molecule is monoclinic (C_2) according to the structure proposed as the most probable one by Ziegler *et al.*[17] The twofold axis, which is parallel to a [100] axis of the average tetragonal structure, must be a principal axis of the g tensor by symmetry considerations.[18] For the second (less probable) structure the point symmetry of the O_2^- site is triclinic. There would be in a domain two orientations of the O_2^- molecules, which transform into each other by a glide plane. However, the two orientations of the g tensor cannot be resolved, because the strong exchange interaction averages the two tensors.[19] Then, one principal axis of the average g tensor is perpendicular to the glide plane, which corresponds to a [100] axis of the average tetragonal cell just as for the first structure. For both possibilities the rotation of the static magnetic field in a tetragonal (100) plane yields the other two principal axes. Figure 7(a) shows the orientation of the principal axes for one of the four domains. The other orientations are obtained by 90° rotations around the [001] axis. The z axis of the g tensor is very close to the average molecular orientation as will be shown in Sec. IV B 3. The determination of this axis gives a much more accurate orientation of the molecular axis than x-ray diffraction. At $T=13.0$ K the angle α between the z axis and the [001] axis is $21.8° \pm 0.5°$. At $T=78$ K one finds $\alpha=18.9° \pm 0.5°$.

The inset of Fig. 6 shows the four orientations of the g tensor present in a twinned crystal using the projection given in Fig. 7(b). The intensities of the four lines are not equal due to different volume fractions of the four domains. For different cooling runs the ratio of the intensities of line No. 2 to line No. 4 differs, whereas the ratio of the combined intensity of lines No. 2 and 4 to the combined intensity of

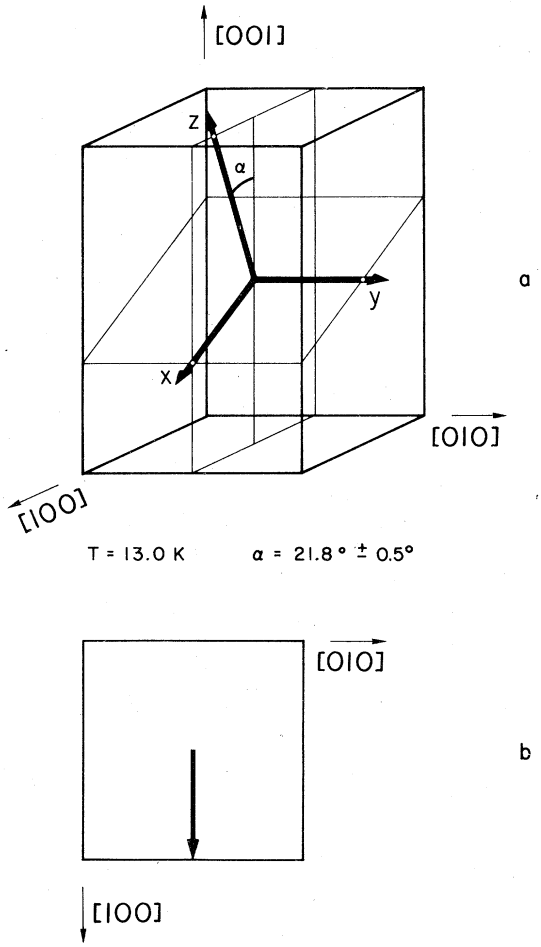

FIG. 7. (a) Orientation of the principal axes at the g tensor of one domain in KO_2 IV referred to the average tetragonal cell. (b) Symbolic sketch of the orientation in (a) [projection of the z axis on the (001) plane], as used in the inset of Fig. 6.

lines No. 1 and 3 remains constant. (For the most thoroughly investigated sample, crystal No. 11, it was equal to about two.) This permits the conclusion that the domains No. 2 and 4 originate from one of the (two) orthorhombic domains at room temperature, whereas the domains No. 1 and 3 arise from the other.

In phase V the crystallographic structures of phases IV and VI coexist.[11] Taking eight crystallographic domains in phase VI and four domains in phase IV (according to x-ray diffraction) there should be up to 12 EPR lines in the spectra. The linewidth prevents complete resolution, and only the peaks of the strongest lines emerge. The ratio of crystal volume having the structure of phase IV to crystal volume having the structure of phase VI is about $\frac{1}{2}$ at $T=10$ K, and it decreases with decreasing temperature until

it is zero at 7 K. The EPR linewidth drops by a factor of about 1.5 at the phase transition IV → V (see Sec. IV B 4). One then estimates that at $T = 9.0$ K the height of the derivative signal corresponding to domains with the crystallographic structure of phase VI should be about four times the height of the signal corresponding to domains with the structure of phase IV. The factor 4 indicates that the observed peaks correspond to domains with the crystallographic structure of phase VI.

The following model explains the EPR spectra as shall be discussed using the data from crystal No. 11 (Fig. 8). There are eight different orientations of the g tensor. One of them is shown in Fig. 9(a). The others can be obtained by applying all symmetry operations of the average tetragonal cell as is indicated in the inset to Fig. 8. A careful analysis of the angular dependence of the spectra including the intensities leads to the conclusion that each orientation corresponds to a different domain. The intensity of a primed line is about half the intensity of an unprimed line. The primed orientations originate from the domains No. 1 and 3 of phase IV and the unprimed orientations from the domains No. 2 and 4. The angle α between the z axis and the g tensor and the [001] axis increases slightly during cooling from 29.5° ±0.5° at 9.0 K to 32.1° ±1.0° at 7 K. The angle ϕ and β (Fig. 9) remain constant within the experimental accuracy, which, however, becomes worse when the Néel temperature is approached because the linewidth increases (see Sec. IV B 4).

The thermal hysteresis of the phase transition IV ↔ V has also been observed.

3. *Principal values of the g tensor*

a. Analysis of the experimental results. The temperature dependence of the resonance field H_0 has been measured along the principal axes between the Néel temperature and liquid-nitrogen temperature. In order to determine the g value the resonance field has to be corrected for internal fields. Following Kötzler and Scheithe[20] one obtains in case of the magnetic field parallel to the z axis

$$H_0^z = \frac{\hbar\omega}{g_z^* \mu_B} \frac{\chi_x + \chi_y}{2\chi_z} , \quad \text{or} \quad g_z^* = g_z \frac{\chi_x + \chi_y}{2\chi_z} , \tag{9}$$

where (within the MFA)

$$\chi_\alpha = \frac{C}{T - \Theta_\alpha + N_\alpha C} \quad (\alpha = x,y,z) .$$

g_z^* is the true g value, g_z is the measured (effective) g value, Θ_α the Curie-Weiss temperature [Eq. (6)],

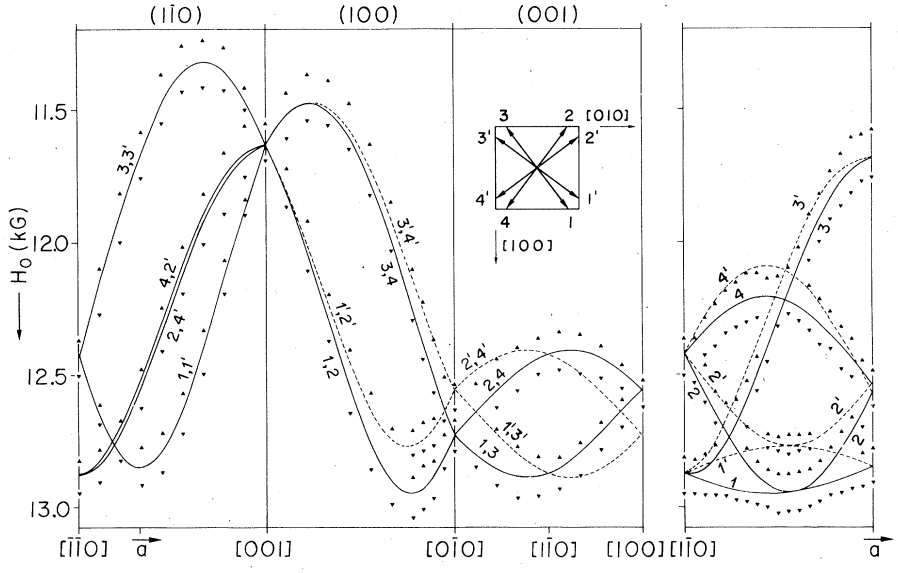

FIG. 8. Angular dependence of the resonance fields in KO_2 V for different planes. {$\vec{a}$ lies in the (1$\bar{1}$0) plane and includes an angle of 28.5° with the [$\bar{1}$10] axis.} The solid and broken lines are the calculated resonance fields based on the model described in the text. Measurements of crystal No. 11 at $T = 9.0$ K: ▲ maximum of the first derivative of the absorption line, ▼ minimum of the first derivative of the absorption line. (The intensity of the unprimed lines 1, 2, 3, and 4 is about twice the intensity of the primed lines 1', 2', 3', and 4'.) $\nu = 35.4$ GHz.

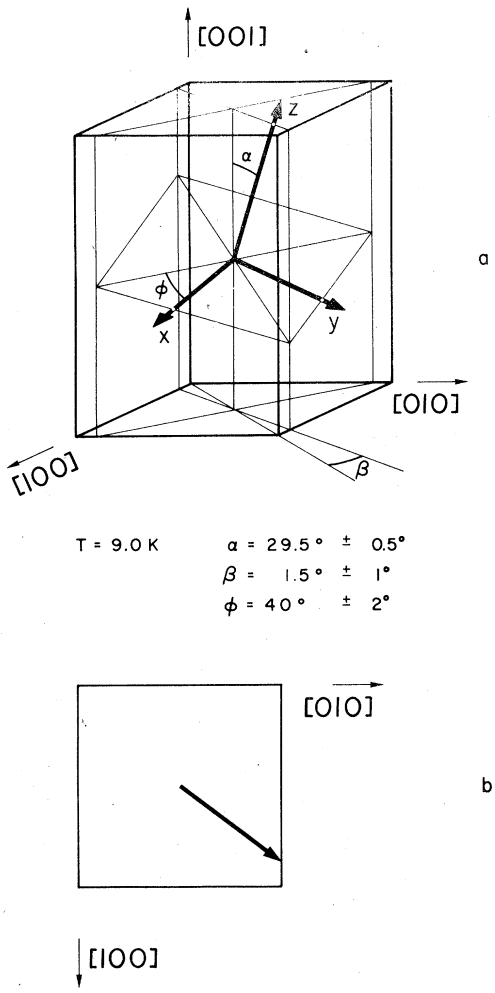

FIG. 9. (a) Orientation of the principal axes of the g tensor of one domain in KO_2 V referred to the average tetragonal cell. (b) Symbolic sketch of the orientation in (a) [projection of the z axis on the (001) plane], as used in the inset of Fig. 8.

and N_α is the demagnetization factor. If the anisotropy of the Curie-Weiss temperature is small one has

$$\frac{\chi_x+\chi_y}{2\chi_z} \cong 1+\tfrac{3}{2}(N_z-\tfrac{1}{3}(4\pi)+\tfrac{1}{2}P_z)\frac{C}{T-\Theta} \quad , \qquad (10)$$

where $\Theta=-\frac{1}{2}C(A+\Gamma)$. The relations $N_x+N_y+N_z=4\pi$ and $P_x+P_y+P_z=0$ were used. There are corresponding formulas for the magnetic field parallel to the x and y axis. The typical shape and size of the KO_2 crystals was a right parallelepiped of $0.6\times0.6\times0.2$ mm^3. For the calculation of the demagnetization shift we approximate the crystals by

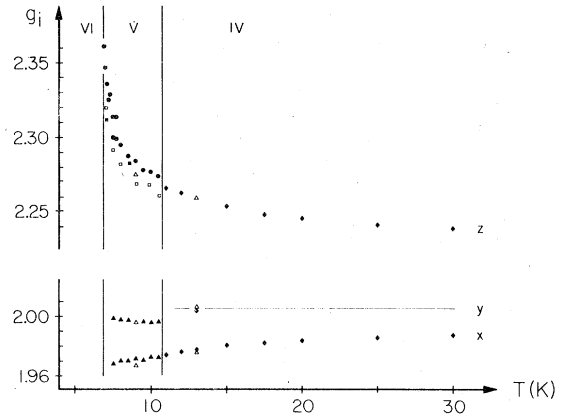

FIG. 10. Temperature dependence of the principal g values of KO_2 corrected for demagnetization but not for anisotropy of the mean-field parameters (several samples).

ellipsoids with principal axes equal to the edges of the parallelepiped. In Fig. 10 the principal g values are plotted as a function of temperature corrected for demagnetization only but not yet for the anisotropy of the mean-field parameters.

In phase IV the temperature dependence of the g tensor can be attributed to the anisotropy of the mean-field parameters as is shown through the following steps. A plot of g_i $(i=x,y,z)$ vs $1/(T-\Theta)$ $(\Theta=+2.3$ K, see Ref. 7) yields a linear function from which one extracts by means of Eq. (9) and (10)

$$g_x^*=1.991\pm0.005\ , \quad P_x=8.1\pm1\ ,$$

$$g_y^*=2.015\pm0.005\ , \quad P_y=6.4\pm1\ ,$$

$$g_z^*=2.231\pm0.005\ , \quad P_z=-15.5\pm2\ .$$

Within experimental accuracy one obtains $P_x+P_y+P_z=0$ which confirms the interpretation. If the temperature dependence of the g's were attributed to a change in the crystal-field splitting, this relation would not hold.

In phase V shifts of the resonance field arising from short-range order manifest themselves. g_z increases more rapidly with decreasing temperature than would be expected from mean-field theory, and it seems to diverge at the Néel temperature. The shift of g_x and g_y cannot be determined, because the lines overlap too much near the Néel temperature as a result of the increasing linewidth. The effect of short-range order on the g value has been studied for one- and two-dimensional systems only (see, e.g., Refs. 21-24). KO_2 behaves similarly. The short-range order invalidates the mean-field analysis for phase V preventing a determination of the parameters P_α. However, the continuity of g_z at the phase transition IV $\leftrightarrow$ V justifies the assumption that the

principal values of the true g tensor in phase V do not differ considerably from those in phase IV, although there is a large change in the molecular orientation. (Compare Figs. 7 and 9.)

b. Theory of the g tensor. A calculation of the principal values of the g tensor of the O_2^- ion in a crystal field of orthorhombic symmetry D_{2h} is given in Ref. 1. Covalent bonding to neighboring ions is taken into account by starting with orthorhombic functions $|\Gamma_2^+\rangle$, $|\Gamma_4^+\rangle$, and $|\Gamma_1^+\rangle$ instead of the corresponding free-ion functions $|\Pi_g^x\rangle$, $|\Pi_g^y\rangle$, and $|\Sigma_g^+\rangle$. The crystal field splits the $^2\Pi_g$ level of the free molecule into $^2\Gamma_2^+$ and $^2\Gamma_4^+$ [see Fig. 11(b)]. The energy difference between the ground state $^2\Gamma_2^+$ and the excited state $^2\Gamma_1^+$ is designated by E. The following matrix elements of the angular momentum and of the spin-orbit interaction $\mathcal{H}_{LS}=-\lambda\vec{L}\cdot\vec{S}$ are nonzero and define the parameters l_i and λ_i $(i=x,y,z)$:

$$\begin{aligned}
&\langle\Gamma_4^+|L_z|\Gamma_2^+\rangle = il_z\ , \quad \langle\Gamma_4^+|\mathcal{H}_{LS}|\Gamma_2^+\rangle = -i\lambda_z S_z\ ,\\
&\langle\Gamma_2^+|L_y|\Gamma_1^+\rangle = il_y\ , \quad \langle\Gamma_2^+|\mathcal{H}_{LS}|\Gamma_1^+\rangle = -i\lambda_y S_y\ ,\\
&\langle\Gamma_1^+|L_x|\Gamma_4^+\rangle = il_x\ , \quad \langle\Gamma_1^+|\mathcal{H}_{LS}|\Gamma_4^+\rangle = -i\lambda_x S_x\ .
\end{aligned} \tag{11}$$

The deviation of l_z from unity is a measure of the orthorhombic distortion of the wave functions. Because λ is of the same order as the crystal-field parameter Δ, the calculation of the wave functions $|\Psi_0\rangle$ corresponding to the (spin-degenerate) ground state was performed exactly in λ/Δ and to first order in λ/E. One then has

$$\begin{aligned}
|\Psi_0\uparrow\rangle &= \cos\alpha|\Gamma_2^+,\uparrow\rangle + i\sin\alpha|\Gamma_4^+,\uparrow\rangle\\
&\quad + \frac{1}{2E}(\lambda_y\cos\alpha - \lambda_x\sin\alpha)|\Gamma_1^+,\downarrow\rangle\ ,\\
|\Psi_0\downarrow\rangle &= \cos\alpha|\Gamma_2^+,\downarrow\rangle - i\sin\alpha|\Gamma_4^+,\downarrow\rangle\\
&\quad - \frac{1}{2E}(\lambda_y\cos\alpha - \lambda_x\sin\alpha)|\Gamma_1^+,\uparrow\rangle\ .
\end{aligned} \tag{12}$$

α is defined by $\tan 2\alpha = \lambda_z/\Delta\ (0\leq\alpha\leq\frac{1}{4}\pi)$. The eigenvalues of the Zeeman energy within this ground-state doublet yield the principal values of the g tensor

$$\begin{aligned}
g_x &= g_0\cos 2\alpha + \frac{l_x}{E}[\lambda_y\sin 2\alpha - \lambda_x(1-\cos 2\alpha)]\ ,\\
g_y &= g_0\cos 2\alpha + \frac{l_y}{E}[\lambda_y(1+\cos 2\alpha) - \lambda_x\sin 2\alpha]\ ,\\
g_z &= g_0 + 2l_z\sin 2\alpha\ .
\end{aligned} \tag{13}$$

z is the orientation of the molecular axis. Assuming $l_x=l_y=l_\perp$ and $\lambda_x=\lambda_y=\lambda_\perp$ only three parameters l_z, α, and $l_\perp\lambda_\perp/E$ are left and these can be calculated from the measured g tensor. This theory explains the g tensor of the O_2^- center in at least eight alkali halides.

This calculation is now extended to monoclinic symmetry C_{2h} in order to study the effect of monoclinic distortion. The orthorhombic y axis is taken as the twofold monoclinic axis. The orthorhombic functions $|\Gamma_2^+\rangle$, $|\Gamma_4^+\rangle$, and $|\Gamma_1^+\rangle$ are replaced by the corresponding monoclinic functions $|1\Gamma_1^+(m)\rangle$, $|\Gamma_2^+(m)\rangle$, and $|2\Gamma_1^+(m)\rangle$ (m stands for monoclinic). Then new nonzero matrix elements appear, namely,

$$\begin{aligned}
&\langle\Gamma_2^+(m)|L_x|1\Gamma_1^+(m)\rangle = i\delta_x\ ,\\
&\langle\Gamma_2^+(m)|-\lambda L_x S_x|1\Gamma_1^+(m)\rangle = -i\lambda_x' S_x\ ,\\
&\langle 2\Gamma_1^+(m)|L_z|\Gamma_2^+(m)\rangle = i\delta_z\ ,\\
&\langle 2\Gamma_1^+(m)|-\lambda L_z S_z|\Gamma_2^+(m)\rangle = -i\lambda_z' S_z\ ,
\end{aligned} \tag{14}$$

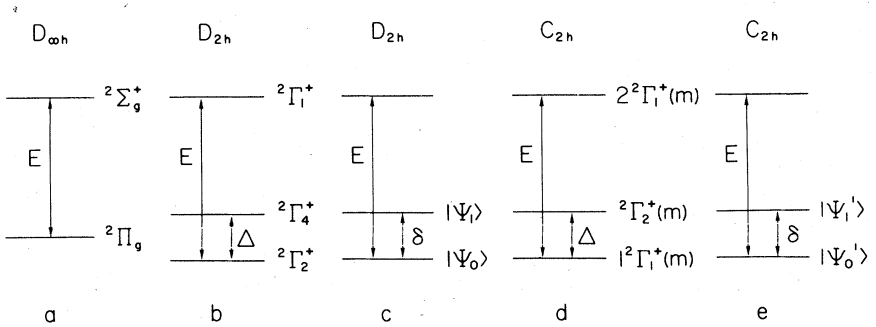

FIG. 11. Energy level scheme of the O_2^- molecule ion for surroundings of different symmetry. $\delta=(\lambda^2+\Delta^2)^{1/2}$. (a) free molecule ion ($D_{\infty h}$). (b) O_2^- in orthorhombic symmetry D_{2h}, spin-orbit interaction neglected. (c) O_2^- in orthorhombic symmetry D_{2h}, spin-orbit interaction taken into account. (d) O_2^- in monoclinic symmetry C_{2h}, spin-orbit interaction neglected. (e) O_2^- in monoclinic symmetry C_{2h}, spin-orbit interaction taken into account.

in addition to those, that existed already for D_{2h} symmetry

$$\begin{aligned}
&\langle\Gamma_2^+(m)|L_z|1\Gamma_1^+(m)\rangle = il_z \ , \\
&\langle\Gamma_2^+(m)|-\lambda L_z S_z|1\Gamma_1^+(m)\rangle = -i\lambda_z S_z \ , \\
&\langle 1\Gamma_1^+(m)|L_y|2\Gamma_1^+(m)\rangle = il_y \ , \\
&\langle 1\Gamma_1^+(m)|-\lambda L_y S_y|2\Gamma_1^+(m)\rangle = -i\lambda_y S_y \ , \\
&\langle 2\Gamma_1^+(m)|L_x|\Gamma_2^+(m)\rangle = il_x \ , \\
&\langle 2\Gamma_1^+(m)|-\lambda L_x S_x|\Gamma_2^+(m)\rangle = -i\lambda_x S_x \ .
\end{aligned} \tag{15}$$

In the framework of perturbation theory one can write

$$\begin{aligned}
|1\Gamma_1^+(m)\rangle &= |\Pi_g^x\rangle + a|\Sigma_g^+\rangle \ , \\
|\Gamma_2^+(m)\rangle &= |\Pi_g^y\rangle \ , \\
|2\Gamma_1^+(m)\rangle &= |\Sigma_g^+\rangle + b|\Pi_g^x\rangle \ ,
\end{aligned} \tag{16}$$

where a and b are of the order of Δ/E. Therefore δ_x and δ_z are of the same order and λ_x' and λ_z' are of the order $\lambda\Delta/E$. The calculation is again performed exactly in λ/Δ and to first order in λ/E and λ'/Δ, neglecting terms of the order λ'/E. The ground-state functions are

$$\begin{aligned}
|\Psi_0'\uparrow\rangle &= \cos\alpha|1\Gamma_1^+(m),\uparrow\rangle + i\sin\alpha|\Gamma_2^+(m),\uparrow\rangle + \frac{1}{2E}(\lambda_y\cos\alpha - \lambda_x\sin\alpha)|2\Gamma_1^+(m),\downarrow\rangle \\
&\quad + \frac{\lambda_x'}{2\Delta}\cos 2\alpha[\sin\alpha|1\Gamma_1^+(m),\downarrow\rangle + i\cos\alpha|\Gamma_2^+(m),\downarrow\rangle] \ , \\
|\Psi_0'\downarrow\rangle &= \cos\alpha|1\Gamma_1^+(m),\downarrow\rangle - i\sin\alpha|\Gamma_2^+(m),\downarrow\rangle - \frac{1}{2E}(\lambda_y\cos\alpha - \lambda_x\sin\alpha)|2\Gamma_1^+(m),\uparrow\rangle \\
&\quad - \frac{\lambda_x'}{2\Delta}\cos 2\alpha[\sin\alpha|1\Gamma_1^+(m),\uparrow\rangle - i\cos\alpha|\Gamma_2^+(m),\uparrow\rangle] \ .
\end{aligned} \tag{17}$$

From there one calculates the principal values of the g tensor. The expressions for g_x and g_z differ from those for orthorhombic symmetry only in terms of the order $(\lambda/E)^2$. The formula for g_y is the same as for the orthorhombic case. Therefore one expects that the monoclinic distortion does not manifest itself measurably in the principal values of the g tensor. The calculation yields, however, an estimate of the deviation of the principal axis z from the internuclear axis of the O_2^- molecule ion. It is of the order of Δ/E. The actual point symmetry of the O_2^- ion in phase IV of KO_2 is C_2 and not C_{2h}. However, the additionally appearing nonzero matrix elements are very small and do not influence the qualitative discussion given for C_{2h} symmetry.

One is led to expect that expressions (13) for the principal values of the g tensor for orthorhombic symmetry can be applied to the alkali hyperoxides. From the (true) g values of KO_2 IV one then obtains the following parameters:

$$l_z = 1.01 \pm 0.02 \ , \quad \tan 2\alpha = \frac{\lambda_z}{\Delta} = 0.11 \pm 0.02$$

and

$$l_\perp\lambda_\perp/E = (13 \pm 2)\times 10^{-3} \ .$$

With $\lambda_z = 180\ \text{cm}^{-1}$, $E = 5\ \text{eV}$,[1] and $\lambda_z/\Delta = 0.11$, one estimates for the angle between the principal axis z and the internuclear axis of the O_2^- molecule a value of about 2°. The parameter $l_\perp\lambda_\perp/E$ is about five times larger in KO_2 than for the O_2^- center in potassium halides.[1] It is difficult to understand this difference, because $l_\perp$, $\lambda_\perp$, and E are quantities that are primarily determined by the properties of the O_2^- ion and are not expected to be strongly influenced by the crystal field. It is conceivable, that due to the interactions between O_2^- molecule ions the treatment of O_2^- in KO_2 as a center is not appropriate. This is also indicated by the fact, that $g_y - g_x$ for an O_2^- ion of the pair in KI (see Ref. 4) is of the of the same magnitude as in KO_2. ($g_y - g_x$ is proportional to $l_\perp\lambda_\perp/E$.)

4. Linewidth

The EPR linewidth of KO_2 has been measured between the Néel temperature (7 K) and 150 K. Some of the results are given in Fig. 12. The shape of the lines is Lorentzian for all orientations of the static magnetic field and for all temperatures. In phase IV ($T \geq 11$ K) the linewidth does not depend on temperatures up to about 80 K. For the static magnetic field applied parallel to the z axis of the g tensor it amounts to 195 ± 10 G (peak to peak of the first derivative of the absorption signal) and parallel to the x axis to 163 ± 10 G. Parallel to the y axis linewidth data cannot be taken because the line coincides with the lines of two other domains (see Sec. IV B 2). The temperature independence of the linewidth is due to exchange narrowing of a line

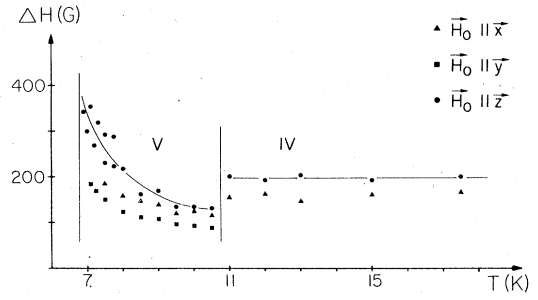

FIG. 12. EPR linewidth (peak to peak of the derivative) for KO_2 as a function of temperature for the static magnetic field H_0 applied parallel to the principal axes of the g tensor.

broadened by dipole-dipole and anisotropic exchange interactions as will be discussed in Sec. VI.

Above 80 K the onset of a strong broadening is observed. It can be explained by a thermally activated reorientation process of the molecule ions

$$\Delta H(T) = \Delta H(0) + Ae^{-E/kT} , \tag{18}$$

with $A = (1.8 \pm 1) \times 10^5$ G and

$$E = (6 \pm 1) \times 10^{-2} \text{ eV} = 700 \text{ K} .$$

Interpreting the broadening as lifetime broadening one obtains

$$\frac{1}{T_1} = Be^{-E/kT} ,$$

with

$$B = 2.8 \times 10^{12} \text{ sec}^{-1} \cong 90 \text{ cm}^{-1} .$$

This value of B is typical for libration frequencies in KO_2 at room temperature.[15] E is of the order of the activation energy for reorientations of the O_2^- center in alkali halides.[25–27] Hence $1/T_1$ reflects the reorientation rate of an O_2^- molecule ion. Unfortunately the reorientation mechanism cannot be specified more precisely because the anisotropy of the preexponential factor B could not be measured due to overlap of the different EPR lines.

In phase V the linewidth increases if the Néel temperature is approached. It can be described by the relation

$$\Delta H(T) = \Delta H(\infty) + \Delta H_c(T) ,$$

where

$$\Delta H_c(T) = \alpha[(T - T_N)/T_N]^{-p} . \tag{19}$$

$\Delta H(\infty)$ is equal to 110, 85, and 130 ± 10 G for the static magnetic field parallel to the x, y, and z axis, respectively. The critical exponent p is about unity. The temperature-independent term $\Delta H(\infty)$ can again be interpreted by exchange narrowing. The temperature-dependent contribution $\Delta H_c(T)$ is due to critical fluctuations. In antiferromagnets these cause a broadening at the approach of the critical temperature, whereas in ferromagnets a narrowing occurs.[28] The temperature dependence of the linewidth thus indicates in agreement with neutron-diffraction[8] and static magnetic susceptibility data,[7] that the Néel temperature T_N of KO_2 is indeed at 7 ± 1 K. The anomaly of the specific heat[7] yields a more accurate value of $T_N = 7.1 \pm 0.1$ K. A detailed study of the critical behavior of the linewidth was not attempted because of the complexity of KO_2. However, it is worth mentioning that the ratio of the critical broadening parallel to the z axis to the critical broadening perpendicular to the z axis is equal to two, just as for a simple uniaxial antiferromagnet.

C. RbO_2

1. *g tensor*

The EPR was studied between the Néel temperature (15 K) and about 40 K. Since the available single crystals are very small (typically $0.3 \times 0.3 \times 0.5$ mm^3) and the linewidth is large and increases with increasing temperature, the signal is too weak at higher temperatures for an accurate investigation. Below 40 K the structure of RbO_2 is pseudo-orthorhombic with a slight monoclinic distortion.[11] The O_2^- molecules are not exactly parallel to each other and therefore the measured g tensor has to be considered as an average over different orientations. (The averaging is achieved by the exchange interaction.) The [001] axis is a twofold axis and common to all domains. It is a principal axis of the average g tensor. The temperature dependence of the resonance field along this axis is given in Fig. 13. At 18 K

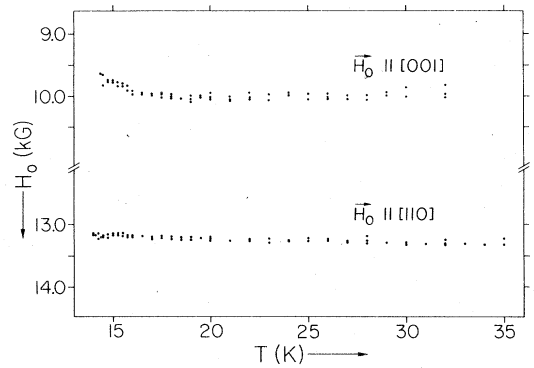

FIG. 13. Temperature dependence of the paramagnetic resonance field H_0 for RbO_2 with the static magnetic field applied parallel to the [001] and the [110] axis of the average tetragonal structure. $\nu = 35.4$ GHz.

it corresponds to a g value of $g_z = 2.534 \pm 0.01$. It is the largest of the principal values and therefore has to be interpreted as corresponding to the average orientation of the molecular axis. Within experimental accuracy no anisotropy of the resonance field was detected in the (001) plane, which means that g_x and g_y differ very little. A measurement of the g value in a (001) plane therefore yields a $g_\perp$. We assume $g_\perp = \frac{1}{2}(g_x + g_y)$. The resonance field parallel to [110] as a function of temperature is given in Fig. 13. At 18 K it corresponds to a g value $g_\perp = 1.915 \pm 0.01$.

The temperature range where accurate measurements are possible is too small for $\vec{H}_0 \| [001]$ to obtain g_z^* and P_z by a fit to formula (9). Fortunately the linewidths are smaller for $\vec{H}_0 \| [110]$, and one obtains

$$g_\perp^* = 1.88 \pm 0.02 = \tfrac{1}{2}(g_x^* + g_y^*)$$

and

$$P_\perp = -120 \pm 50 = \tfrac{1}{2}(P_x + P_y) \ .$$

Since $P_x + P_y + P_z = 0$ one has

$$P_\parallel = P_z = -2P_\perp = +240 \pm 100$$

and

$$g_\parallel^* = g_z^* = g_z\left(1 + \frac{3}{4} P_z \frac{C}{T - \Theta}\right) = 2.63 \pm 0.03 \ .$$

The contribution from demagnetization is included in the P's. It is small because the shape of the crystals deviates little from a cube. Near the Néel temperature the resonance field parallel to [001] decreases more rapidly than would be expected from mean-field theory, as in KO_2. Presumably this is again due to short-range order.

The formulas (13) for the g tensor yield

$$g_\parallel^* = g_z = g_e + l_z \sin 2\alpha \ , \tag{20}$$

$$g_\perp^* = \frac{g_x + g_y}{2} = g_e \cos 2\alpha + \frac{l_\perp \lambda_\perp}{E} \cos 2\alpha \ .$$

The term $(l_\perp \lambda_\perp / E) \cos 2\alpha$ can be neglected because it is smaller than the error of $g_\perp^*$. One then obtains

$$\frac{\lambda_z}{\Delta} = \tan 2\alpha = 0.37 \pm 0.03$$

and

$$l_z = 0.9 \pm 0.1 \ .$$

The crystal-field parameter Δ is much smaller than for KO_2. This can be understood on the basis of the following qualitative arguments. The lattice of RbO_2 is almost tetragonal and the average orientation of the internuclear axis of the O_2^- molecule is parallel to the pseudotetragonal axis. Therefore the crystal field seen by an electron in a Γ_2^+ state (Π_g^x) is very close to that seen by an electron in a Γ_4^+ state (Π_g^y). In contrast to this in KO_2 the surroundings differ more for the two states due to the tilt of the molecular axis, and the crystal-field parameter Δ is larger than for RbO_2.

2. Linewidth

The measurements of the linewidth as a function of temperature are plotted in Fig. 14 for the static magnetic field applied along the [001] and the [110] axis. The line shape is Lorentzian at 18 K for all orientations of the crystal. At other temperatures it was difficult to accurately measure the line shape due to the huge linewidth and the poor signal-to-noise ratio. Within the rather large experimental error it is Lorentzian. We assume three contributions to the linewidth: a temperature-independent term, a term that increases with increasing temperature and a broadening near the Néel temperature;

$$\Delta H = A + \frac{B}{e^{E/kT} - 1} + C\left(\frac{T - T_N}{T_N}\right)^{-p} \ . \tag{21}$$

The temperature-independent term A represents the linewidth left after exchange narrowing of the line broadened by anisotropic spin-spin interactions. It amounts to $A_\parallel = 2100 \pm 400$ G for the static magnetic field parallel to [001] and to $A_\perp = 1200 \pm 400$ G parallel to [110]. It is discussed in Sec. VI.

The second term can be interpreted as lifetime broadening due to a thermally activated reorientation process of the molecule ion. The activation energy is about 80 K. An accurate determination was not possible leaving the temperature-independent term with a large error. The activation energy is considerably smaller than for KO_2. A second interpretation as lifetime broadening due to a Raman process involving optical phonons[29] is also conceivable. A phonon

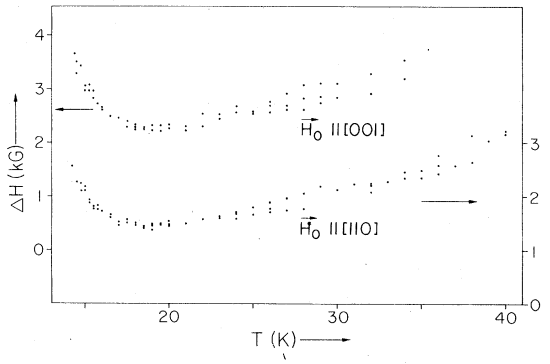

FIG. 14. EPR linewidth ΔH (peak to peak of the derivative) for RbO_2 as a function of temperature with the static magnetic field parallel to the [001] axis (left scale) and the [110] axis (right scale) of the average tetragonal structure.

energy of 80 K = 56 cm^{-1} corresponds to a typical libration frequency in the alkali hyperoxides.[15] For such a process $1/T_1$ is inversely proportional to the fourth power of the crystal-field splitting Δ. Δ can be derived from the g tensor. Comparing KO_2 with RbO_2 one finds that $1/T_1$ is two orders of magnitude smaller for KO_2. Hence, this process cannot be observed in KO_2.

The third term describes the broadening caused by critical fluctuations near the Néel temperature. The broadening confirms the onset of antiferromagnetic order in RbO_2 at about 15 K.[28] The critical exponent is of the order of unity. The accuracy of the EPR measurement is so much limited by the large linewidth that the transitions III → IV (15.1 K) and IV → V (14.7 K) cannot be distinguished.

D. CsO_2

1. g tensor

The EPR was investigated between the Néel temperature (9.6 K) and about 70 K. The spectra show axial symmetry about [001] as for RbO_2. The interpretation is analogous. The resonance field parallel and perpendicular to [001] as a function of temperature is given in Fig. 15. At 15 K it corresponds to an effective g value of $g_{\parallel} = 2.660 \pm 0.01$ and $g_{\perp} = 1.897 \pm 0.005$ parallel and perpendicular to the [001] axis, respectively. After correction for internal fields and demagnetization as described in Sec. IV B 3 one finds

$$g_{\parallel}^{*} = 2.61 \pm 0.02 \ , \quad P_{\parallel} = -130 \pm 50 \ ,$$

and

$$g_{\perp}^{*} = 1.91 \pm 0.01 \ , \quad P_{\perp} = +50 \pm 30 \ .$$

The typical shape of the crystals was a slightly elongated octahedron. The corresponding anisotropy of the demagnetization fields is included in the P's. The parameters determined using formulas (20) are

$$\lambda_z/\Delta = 0.31 \pm 0.02$$

and

$$l_z = 1.01 \pm 0.03 \ .$$

They are close to those for RbO_2 and can be interpreted along the same lines (see Sec. IV C 1).

2. Linewidth

The measured linewidth of CsO_2 parallel and perpendicular to [001] is plotted in Fig. 16. The shape of the line is Lorentzian for all orientations and all temperatures. At 12.5 K the spectra were carefully examined for an anisotropy in a plane perpendicular to [001]. Within experimental accuracy, limited by a signal-to-noise ratio of about 100, all spectra were identical at least in the range of investigation ($|H - H_0| \lesssim 3.5\Delta H$). This limits the difference between g_x and g_y to less than 0.01. Qualitatively the temperature dependence of the linewidth is the same as for RbO_2. The temperature-independent contribution amounts to $A_{\parallel} = 820 \pm 100$ G and $A_{\perp} = 620 \pm 100$ G. The broadening at high temperatures corresponds to an activation energy of about 60 K. The interpretation can be taken over from RbO_2 (see Sec. IV C 2). The broadening at low temperatures confirms the position of the Néel point near 9 K.

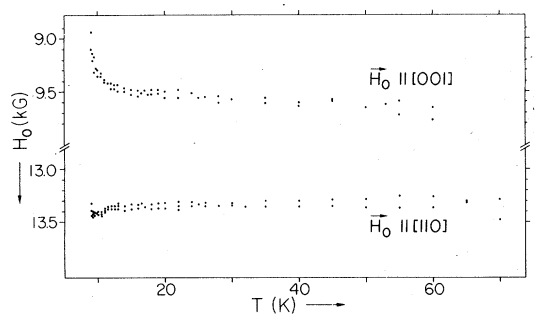

FIG. 15. Temperature dependence of the paramagnetic resonance field H_0 for CsO_2 with the static magnetic field applied parallel to the [001] and the [110] axis of the average tetragonal structure. $\nu = 35.4$ GHz.

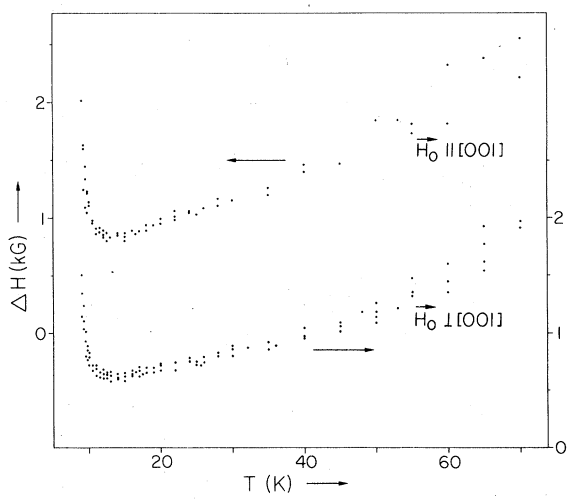

FIG. 16. EPR linewidth ΔH (peak to peak of the derivative) for CsO_2 as a function of temperature with the static magnetic field parallel (left scale) and perpendicular (right scale) to the [001] axis of the average tetragonal structure.

V. ANTIFERROMAGNETIC RESONANCE

A. Theoretical considerations

There are two mechanisms for the absorption of infrared radiation in the ordered state of an antiferromagnet: Magnetic-dipole transitions occur by creation of one magnon of wave vector $k=0$ and electric-dipole transitions by simultaneous creation of a magnon with arbitrary wave vector k and a magnon with wave vector $-k$.

The one magnon processes can be described by the mean-field approximation. Since $k=0$, all spins within a sublattice precess in phase. Date[30] calculated the frequencies for a mean-field energy of the form (2). Defining x as the easy, y as the intermediate, and z as the hard axis one finds for the frequencies of the $k=0$ magnons for $\vec{H}\parallel\vec{y}$ under the assumptions $|P_\alpha| \ll |A|$ and $|Q_\alpha| \ll |A|$ $(\alpha=x,y,z)$ justified in Sec. III, and with $\chi_y = 1/(A+\frac{1}{2}P_y)$,

$$\text{I.}\quad \left(\frac{\omega}{\gamma}\right)^2 = H^2(1-\tfrac{3}{2}P_y\chi_y)+2(Q_x-Q_y)AM_0^2 \quad (22)$$

and

$$\text{II.}\quad \left(\frac{\omega}{\gamma}\right)^2 = H^2\frac{Q_xQ_z}{4}\chi_y^2+2(Q_x-Q_z)AM_0^2 \quad . \quad (23)$$

$H=\frac{1}{2}g_y^*H_{ex}$ is the reduced field and M_0 is the magnetization of a sublattice. Mode I (Eq. 22) is (elliptically) polarized in the x-z plane whereas Mode II (Eq. 23) is (linearly) polarized parallel to the y axis. For the magnetic field H parallel to the z axis the frequencies are given by

$$\text{III.}\quad \left(\frac{\omega}{\gamma}\right)^2 = H^2(1-\tfrac{3}{2}P_z\chi_z)+2(Q_x-Q_z)AM_0^2 \quad (24)$$

and

$$\text{IV.}\quad \left(\frac{\omega}{\gamma}\right)^2 = H^2\frac{Q_xQ_y}{4}\chi_z^2+2(Q_x-Q_y)AM_0^2 \quad , \quad (25)$$

where $\chi_z=1/(A+\frac{1}{2}P_z)$ and $H=\frac{1}{2}g_z{}^*H_{ex}$. Mode III (Eq. 24) is (elliptically) polarized in the x-y plane and Mode IV (Eq. 25) is (linearly) polarized parallel to the z axis. The zero-field frequency of Mode I is smaller than that of Mode III because $Q_x > Q_y > Q_z$. For H parallel to the x axis (easy) the field dependence of the magnon frequencies is more complicated.

The absorption due to two magnon processes is weighted by the magnon density of states. Therefore the absorption band is peaked at energies $2\hbar\omega(k)$ whose wave vector k belongs to special points at the Brillouin-zone boundary.[31] The magnon frequency $\omega(k_{ZB})$ at the zone boundary can be estimated using a relation derived in Ref. 14

$$\hbar\omega(k_{ZB}) \approx zJS = Ng_0^2\mu_B^2S(A+\Gamma) \quad . \quad (26)$$

Inserting values for N, A, and Γ for the alkali hyperoxides one obtains for the energy $2\hbar\omega(k_{ZB})$ of the two magnon absorption peaks values between 45 and 80 cm^{-1}. A more thorough discussion would involve a detailed calculation of the magnon dispersion. It cannot be carried out because the details of the magnetic structure are not known.

B. Experimental techniques

The far-infrared (far-ir) absorption of KO_2, RbO_2, and CsO_2 has been measured in the frequency range from 2 to 55 cm^{-1} by means of Fourier-transform spectroscopy for temperatures between 1.4 and 60 K. (These experiments were performed by M. A. Bösch at the Laboratory of Atomic and Solid State Physics at Cornell University.) The samples consisted of many small single crystals filled into sample cells of 4 mm diameter and 6.5 or 8 mm length with sapphire or teflon windows. A magnetic field up to 90 kG was applied by means of a superconducting solenoid. The infrared radiation propagates parallel to the magnetic field. The ratio of the absorption spectra taken at different temperatures or at different magnetic fields was analyzed in order to eliminate the spectrum of the radiation source, the spectral sensitivity of the bolometer and intensity variations due to interference. Frequency shifts and intensity changes are thus obtained permitting conclusions about the absorption spectrum of the sample. The magnetic field strength was known within an accuracy of about 3%. The frequency resolution is about 0.3 cm^{-1} in the range from 2 to 15 cm^{-1} and about 1 cm^{-1} between 15 and 55 cm^{-1}.

C. Results

1. CsO_2

At frequencies below 15 cm^{-1} absorption peaks with a strong field dependence of the frequency have been observed. The experimental data for CsO_2 are shown in Fig. 17.

The crystals are loose in the sample cell and they orient so that the easy axis is perpendicular to the magnetic field. Thus referred to the crystal axes the magnetic field lies randomly within a plane perpendicular to the easy axis. Absorption maxima occur at frequencies equal to the magnon frequencies for the magnetic field parallel to the intermediate and hard axis because the angular dependence of the magnon frequencies passes through an extremum at these

axes. The field dependence of the magnon frequencies for the magnetic field parallel to these axes is given by formulas (22) to (25). The full and broken lines in Fig. 17 represent the fit to the experimental data. The nearly field-independent modes II and IV are not excited because their polarizations are parallel to the static magnetic field. However, one observes a coupling between mode I and II because the magnetic field is not exactly parallel to the y axis.[32] The intensity decreases with decreasing field due to the increasing admixture of mode II. The other mode, which is expected from the coupling of I and II, is not detected because at high magnetic fields its character is predominantly that of mode II and at low magnetic fields its frequency is low and lies in the spectral region where accurate measurements are no longer possible.

At $H_{ex}=90$ kG the absorption of mode III, for which the static magnetic field is parallel to the hard axis z, can be followed into the paramagnetic phase, where at 15 K its frequency is 11.2 cm^{-1}. This value corresponds to the EPR g value parallel to the [001] axis of the average tetragonal CaC_2-type cell. Thus one concludes that in CsO_2 the hard axis of magnetization is parallel to the average orientation of the molecular axis. In zero field the frequency of mode III decreases with increasing temperature, and the absorption disappears between 8.2 and 11.2 K. (The Néel temperature is 9.6 K.)

From a fit to formula (24) of the field dependence of the resonance frequency of mode III at $T=1.4$ K

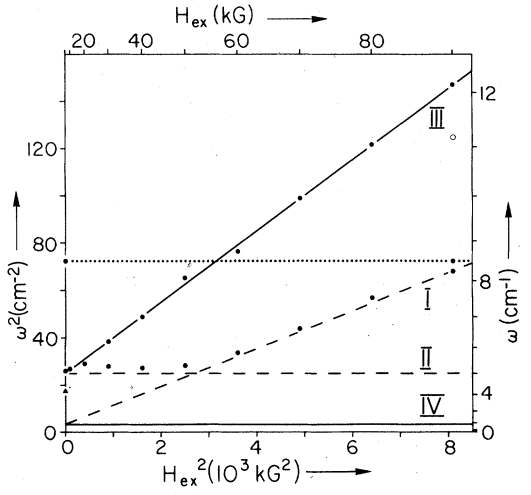

FIG. 17. Absorption peaks in the far infrared for CsO_2 (square of frequency ω vs square of externally applied magnetic field H_{ex}). ●: $T=1.4$ K, ▲: $T=8.2$ K, ○: $T=15.1$ K. Full lines: field dependence of the resonance frequencies for the static magnetic field parallel to the (hard) axis z. Broken lines: field dependence of the resonance frequencies for the static magnetic field parallel to the (intermediate) axis y. Dotted line: nonmagnetic absorption?

one obtains

$$\omega(H=0)=\gamma[2(Q_x-Q_z)A]^{1/2}M_0=5.0\pm0.1\ \text{cm}^{-1}$$

and

$$\tfrac{1}{4}g_z^{*2}(1-\tfrac{3}{2}P_z\chi_z)=1.72\pm0.05\ .$$

Using these data one can determine Q_x-Q_z. A is taken from Sec. III. For M_0 we insert the saturation value $Ng_0\mu_B S$. One finds then $Q_x-Q_z=79$. $1-\frac{3}{2}(P_z\chi_z)$ cannot be determined accurately enough to obtain P_z. However, the value of P_z resulting from the temperature dependence of the EPR resonance field is consistent with the slope of ω^2 vs H_{ex}^2. Extrapolating the measured spin-flop field of Ref. 7 (see Sec. III) to $T=0$ K one obtains $H_{cex}=21.3$ kG. Since the easy axis is perpendicular to the average orientation of the molecular axis the value $g_\perp^*=1.91$ has to be used for the reduction of the spin-flop field. Using formula (8) one computes $Q_x-Q_y=11$. From $Q_x+Q_y+Q_z=0$ one then obtains $Q_x=30$, $Q_y=19$, and $Q_z=-49$. With the P's determined in Sec. IV D 1 and adjusted for a vanishing trace, one finds for the anisotropic mean-field parameters

$$A_x'=45\ ,\quad A_y'=40\ ,\quad A_z'=-85\ ,$$

$$\Gamma_x'=15\ ,\quad \Gamma_y'=20\ ,\quad \Gamma_z'=-35\ .$$

An absorption peak with field- and temperature-independent frequency 8.5 cm^{-1} is present in the spectrum. It is much stronger than the AFMR absorption at zero field. It persists still far above the Néel temperature although its intensity decreases with increasing temperature. A corresponding peak was observed in RbO_2 but not in KO_2. This suggests that it might be connected with the incommensurate crystallographic superstructure.

An absorption band with peaks at 34, 38, and 42.5 cm^{-1} was observed. The intensity decreases with increasing temperature. The peak at 42.5 cm^{-1} is the strongest and the one at 38 cm^{-1} the weakest. A field dependence outside experimental error could not be detected. This absorption band is likely to be due to two magnon processes. The frequencies are of the expected order of magnitude (see Sec. V A).

2. RbO_2

The field dependence of the frequencies at which peaks in the far-ir absorption of RbO_2 occur is shown in Fig. 18. The interpretation presented for CsO_2 can be taken over. At $H_{ex}=90$ kG the absorption of mode III can be followed into the paramagnetic phase where its frequency corresponds to a g value which is equal to the EPR g value parallel to the [001] axis. When (at 90 kG) mode I is followed into the

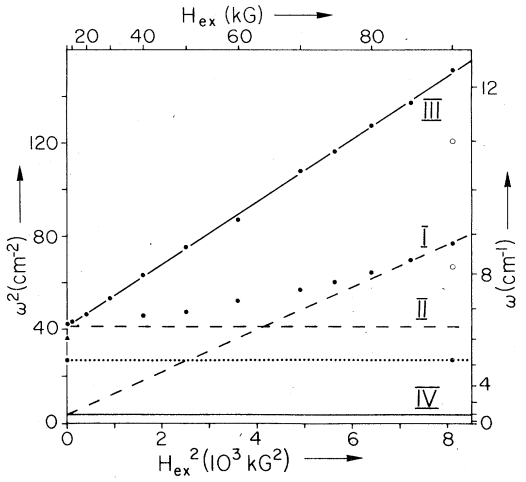

FIG. 18. Absorption peaks in the far infrared for RbO_2 (square of frequency ω vs square of externally applied magnetic field H_{ex}). •: $T=1.5$ K, ▲; $T=12.1$ K, ○: $T=16.1$ K. Full, broken, and dotted lines have the same meaning as in Fig. 17.

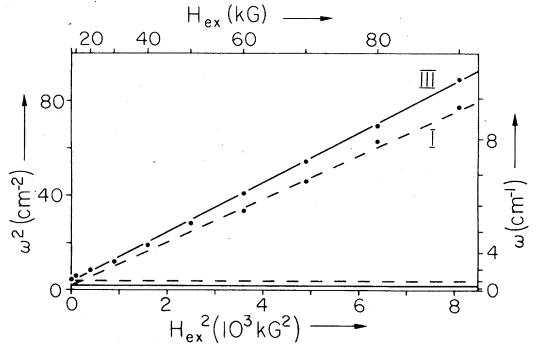

FIG. 19. Absorption peaks in the far infrared for KO_2 at $T=1.4$ K (square of frequency ω vs square of externally applied magnetic field H_{ex}). Full and broken lines have the same meaning as in Fig. 17.

paramagnetic phase the resulting g value agrees with the EPR g value perpendicular to the [001] axis. Thus in RbO_2 the hard axis of magnetization is parallel to the average orientation of the molecular axis as for CsO_2. In zero field the AFMR frequency decreases from 6.5 cm^{-1} at 1.5 K to 6.0 cm^{-1} at 12.1 K. The absorption disappears at about 15 K. The spin-flop field of Ref. 7 extrapolated to $T=0$ K is $H_{cex}=21.7$ kG. Q_x-Q_y and Q_x-Q_z were computed as for CsO_2. One finds $Q_x=36$, $Q_y=27$, and $Q_z=-63$ and with the P's from Sec. IV C 1,

$$A_x'=-42\ ,\quad A_y'=-46\ ,\quad A_z'=+88\ ,$$

$$\Gamma_x'=-78\ ,\quad \Gamma_y'=-74\ ,\quad \Gamma_z'=+152\ .$$

At 5.2 cm^{-1} there is another absorption peak which has exactly the same properties as the 8.5 cm^{-1} peak in CsO_2. At higher frequencies two further absorption peaks were observed, a strong one at 21.5 cm^{-1} with an intensity that increases with increasing temperature and a weak one at 45.5 cm^{-1} with an intensity that decreases with increasing temperature. The frequency of the latter decreases slightly in a magnetic field to about 44.5 cm^{-1} at 90 kG. The temperature dependence of the intensity suggests a two magnon process.

3. KO_2

The far-ir data for KO_2 below 15 cm^{-1} are shown in Fig. 19. The following observations can be explained on the basis of the anisotropy of the g tensor. The separation of the absorption peaks is smaller for KO_2 than for RbO_2 and CsO_2 and it can be resolved for KO_2 only at high magnetic fields. The AFMR frequency in the absence of a magnetic field is smaller than for RbO_2 and CsO_2 as is expected based on relation (7).

For the determination of the mean-field parameters one proceeds as in the case of RbO_2 and CsO_2 and finds $Q_x=6.8$, $Q_y=-1.2$, and $Q_z=-5.6$. $\vec{P}$ could not be measured in phase V and hence the anisotropic mean-field parameters cannot be given. The data of Fig. 19 together with the EPR g tensor indicate that the easy axis of magnetization is perpendicular to the molecular axis. Neutron diffraction leads to the same suggestion.[8]

The two magnon absorption band shows two peaks at 33.5 and 40 cm^{-1} for $H_{ex}=0$ kG. Its intensity decreases with increasing temperature and disappears above the Néel temperature. When a magnetic field of 70 kG is applied at 1.6 K the peak at 33.5 cm^{-1} shifts to about 32 cm^{-1}. The intensity of the whole absorption band decreases with increasing field and disappears abruptly between 70 and 80 kG. This first-order phase transition (see Ref. 7) cannot be identified with the phase transition between the spin-flop phase and the paramagnetic phase, which is second order and would be expected at $H_c'=2AM_0=340$ kG (if one neglects the anisotropic mean-field parameters). It has rather to be interpreted as the field-induced transition to the paramagnetic phase IV. This transition involves a large change of the molecular orientation as was shown in Sec. IV B 2, as well as a deformation of the unit cell.[11]

VI. FURTHER DISCUSSION

In order to test the usefulness of the mean-field parameters of RbO_2 and CsO_2 the computed temperature-independent contribution to the EPR linewidth was compared to the experimental results.

This contribution corresponds to a line broadened by anisotropic spin-spin interactions and subsequently narrowed through exchange. The calculation requires knowledge of the individual spin-spin interactions $\vec{J}_{jk}$. These can be extracted from experimental data under the following simplifying assumptions:

(i) Only the exchange interactions of an ion with its 12 nearest neighbors shall be considered. (Their distances are 4.2 or 4.6 Å in RbO_2 and the distance to farther neighbors is at least 6.0 Å. For KO_2 and CsO_2 the geometrical situation is similar.)

(ii) The spin-spin interactions $\vec{J}$ (isotropic plus anisotropic part) between an ion and its four nearest neighbors in the same (001) plane of the average tetragonal CaC_2-type structure shall be equal. Furthermore the interactions $\vec{J}^*$ between an ion and its eight nearest neighbors in the two adjacent tetragonal (001) planes also shall be equal. (These assumptions are reasonable for the isotropic part of the interactions. However, the equalities are not so realistic for the anisotropic part because the principal axes are not parallel to each other.)

(iii) Adopting the proposal for the magnetic structure of KO_2 given in Ref. 8 we assume that the spins order ferromagnetically within tetragonal (001) planes and the spins in adjacent planes are aligned antiparallel.

Then we have

$$\vec{J} = \tfrac{1}{4} N g_0^2 \mu_B^2 \vec{\Gamma}$$

and

$$\vec{J}^* = \tfrac{1}{8} N g_0^2 \mu_B^2 \vec{A} \quad . \tag{27}$$

The dipole-dipole interaction is included in this treatment. The second moment μ_Ω^2 of the EPR line can be calculated by expressions given in Ref. 33. The nonsecular broadening has to be taken into account. Then according to Ref. 34 the spin-spin relaxation time T_2 arising from exchange narrowing is given by

$$\frac{1}{T_2} = \left(\frac{\pi}{2}\right)^{1/2} \frac{\mu_\Omega^2}{\omega_e} \quad , \tag{28}$$

where (Ref. 35)

$$\omega_e^2 = \tfrac{2}{3} S(S+1) \sum_j \left(\frac{J_{jk}}{\hbar}\right)^2 \quad . \tag{29}$$

For a computation of the linewidth the mean-field parameters given in Secs. III and V C are used. In Table II the results are compared to the measured EPR linewidths. It is striking that the measured linewidths are several times larger than the calculated ones, although some qualitative properties are reproduced. Presumably the origin of this discrepancy lies not in the shortcomings of the mean-field approach but rather in the neglect of important properties of the actual structure of these compounds. The calculation of the exchange narrowing is based on the assumption of a perfect crystalline lattice. This we do not have for RbO_2 and CsO_2. The incommensurate crystallographic superstructure is an indication of incomplete molecular order.

For a comparison of the relative magnitude of the dipole-dipole interaction and the anisotropic part of the exchange interaction the dipole contribution to the anisotropic mean-field parameters was calculated, based on a point dipole model and an orthorhombically distorted CaC_2-type structure.[11] The contribution of the dipole-dipole interaction to $\vec{P}$ does not depend on the magnetic structure. One finds $P_{x,\mathrm{dip}} = -13$, $P_{y,\mathrm{dip}} = -12$, and $P_{z,\mathrm{dip}} = 25$ for RbO_2 and for CsO_2. Comparison with the total $\vec{P}$ given in Secs. IV C 1 and IV D 1 shows that the anisotropy of the spin-spin interaction originates predominantly in the exchange.

For KO_2 the anisotropic mean-field parameters are smaller than for RbO_2 and CsO_2 which manifests itself in narrower EPR lines. A detailed analysis was not possible because the crystallographic changes between the phases IV and VI prevent the determination of a complete set of mean-field parameters for phases V and VI.

VII. CONCLUSIONS

a. Crystallographic information from EPR. In phase IV of KO_2 the analysis of the g tensor yielded the orientation of the O_2^- molecule ions with much greater precision than x-ray diffraction. In phase V, where diffraction methods failed because of the complicated crystallographic domain structure, the EPR spectra permitted the determination of the molecular orientation and gave information on the domain structure.

TABLE II. Calculated and experimental values of the temperature independent part of the EPR linewidth (peak to peak of the derivative).

	ΔH (G) calculated			ΔH (G) experimental (phase III)	
	$\vec{H}_0 \parallel \vec{x}$	$\vec{H}_0 \parallel \vec{y}$	$\vec{H}_0 \parallel \vec{z}$	$\vec{H}_{0\perp}$ [001]	$\vec{H}_0 \parallel$ [001]
RbO_2	440	430	620	1200 ± 400	2100 ± 400
CsO_2	51	51	74	620 ± 100	820 ± 100

In phase III of RbO_2 and CsO_2 the average orientation of the O_2^- molecule ions could be determined.

b. Magnetic structure and interactions. The compounds KO_2, RbO_2, and CsO_2 are antiferromagnetic with Néel temperature 7, 15, and 9 K, respectively, as is indicated by the following observations. Antiferromagnetic resonance occurs below these temperatures. With decreasing temperature the paramagnetic resonance absorption decreases abruptly at these temperatures and the linewidth increases on approaching these temperatures. The knowledge of the g tensor from EPR spectroscopy and of its relation to the internuclear axis of the O_2^- molecule ion combined with the field dependence of the AFMR permitted the determination of the magnetic axes. The easy axis of magnetization is perpendicular to the molecular axis, and the hard axis is parallel to it for all three compounds.

There is a considerable temperature range where short-range order occurs as revealed by the critical behavior of the EPR linewidth and of the EPR resonance field.

On the basis of a mean-field approximation the magnetic interactions were determined using the Néel temperature, the Curie-Weiss temperature, the spin-flop-field, the temperature dependence of the EPR resonance field, and the AFMR frequencies.

ACKNOWLEDGMENTS

Many helpful discussions with Professor F. Waldner, Dr. H. Rohrer, Dr. M. Ziegler, Dr. M. Rosenfeld, M. Rossinelli, B. von Allmen, H. Wahlen, and other members of the Laboratory of Solid State Physics of the Eidgenössische Technische Hochschule are gratefully acknowledged. We also thank H. R. Aeschbach and M. Wächter for technical assistance. This work was supported by the Swiss National Science Foundation. One of us (MAB) acknowledges helpful discussions with Professor A. J. Sievers. The far-ir work was supported by the U. S. Energy Research and Development Administration under Contract No. EY-76-S-02-3151.

---

*Present address: Laboratory of Phys. Chem., Swiss Federal Inst. of Tech., CH-8092 Zürich, Switzerland.

†Present address: Laboratoire de Phys. des Solides, Centre National de la Recherche Scientifique et Univ. de Paris-Sud, 91405 Orsay, France.

‡Present address: Bell Laboratories, Holmdel, New Jersey 07733

[1]H. R. Zeller and W. Känzig, Helv. Phys. Acta 40, 845 (1967).

[2]R. T. Shuey and H. R. Zeller, Helv. Phys. Acta 40, 873 (1967).

[3]K. K. Rebane and L. A. Rebane, Pure Appl. Chem. 37, 161 (1974), and references therein.

[4]R. Baumann, H. U. Beyeler, and W. Känzig, Helv. Phys. Acta 44, 252 (1971).

[5]H. U. Beyeler, R. Baumann, and W. Känzig, Phys. Cond. Matt. 11, 286 (1970).

[6]M. Ziegler, M. Rosenfeld, W. Känzig, and P. Fischer, Helv. Phys. Acta 49, 57 (1976).

[7]A. Zumsteg, M. Ziegler, W. Känzig, and M. Bösch, Phys. Cond. Matt. 17, 267 (1974).

[8]H. G. Smith, R. M. Nicklow, L. J. Raubenheimer, and M. K. Wilkinson, J. Appl. Phys. 37, 1047 (1966).

[9]W. Känzig and M. Labhart, J. Phys. (Paris) 37, C7-39 (1976).

[10]D. E. Cox, E. J. Samuelsen, and. K. H. Beckurts, Phys. Rev. B 7, 3102 (1973).

[11]M. Rosenfeld, M. Ziegler, and W. Känzig, Helv. Phys. Acta 51, 298 (1978).

[12]F. Halverson, J. Phys. Chem. Solids 23, 207 (1962).

[13]T. Moriya, in *Magnetism,* edited by G. T. Rado and H. Suhl (Academic, New York, 1963), Vol. I.

[14]F. Keffer, in *Handbuch der Physik,* edited by S. Flügge (Springer, Berlin, 1966), Vol. XVIII, Part 2.

[15]M. Bösch and W. Känzig, Helv. Phys. Acta 48, 743 (1975).

[16]L. S. Singer and C. Kikuchi, J. Chem. Phys. 23, 1738 (1955).

[17]M. Ziegler, H. R. Meister, and W. Känzig, Helv. Phys. Acta 48, 599 (1975).

[18]G. E. Pake and T. L. Estle, *The Physical Principles of Electron Paramagnetic Resonance* (Benjamin, New York, 1973).

[19]M. Yokota and S. Koide, J. Phys. Soc. Jpn. 9, 953 (1954).

[20]J. Kötzler and W. Scheithe, Phys. Status Solidi B 69, 389 (1975).

[21]K. Nagata and Y. Tazuke, J. Phys. Soc. Jpn. 32, 337 (1972).

[22]K. Nagata, J. Phys. Soc. Jpn. 40, 1209 (1976).

[23]K. Oshima, K. Okuda, and M. Date, J. Phys. Soc. Jpn. 41, 475 (1976).

[24]T. Karasudani and H. Okamoto, J. Phys. Soc. Jpn. 43, 1131 (1977).

[25]G. Pfister and W. Känzig, Phys. Cond. Matt. 10, 231 (1969).

[26]G. Pfister and M. Bösch, J. Phys. Chem. Solids 31, 2699 (1970).

[27]M. Bösch, H. P. Dreyer, J. Muggli, and W. Känzig, Solid State Commun. 12, 1027 (1973).

[28]M. S. Seehra and D. L. Huber, AIP Conf. Proc. 24, 261 (1974).

[29]C. Y. Huang, Phys. Rev. 154, 215 (1967).

[30]M. Date, J. Phys. Soc. Jpn. 16, 1337 (1961).

[31]R. Loudon, Adv. Phys. 17, 243 (1968).

[32]A. S. Borovik-Romanov and L. A. Prozorova, JETP Lett. 4, 39 (1966).

[33]M. Date, H. Yamazaki, M. Motokawa, and S. Tazawa, Prog. Theor. Phys. Suppl. 46, 194 (1970).

[34]R. Kubo and K. Tomita, J. Phys. Soc. Jpn. 9, 888 (1954).

[35]T. Moriya, Prog. Theor. Phys. 16, 23 (1956).